Journal Name

ARTICLE TYPE

Cite this: DOI: 00.0000/xxxxxxxxxx

# Cavity-mediated enhancement of CISS in DNA junctions

Anqi Li[a] and Michael Galperin[b]

Received Date
Accepted Date

DOI: 00.0000/xxxxxxxxxx

Using a model of the double-stranded DNA junction, we employ a nonequilibrium Green's function (NEGF) approach to theoretically study the chiral induced spin selectivity (CISS) effect both outside and inside the molecular cavity. We demonstrate that outside the cavity, spin polarization is sensitive to gate voltage, and we explain this sensitivity through the alternating character of DNA molecular orbitals. Inside the cavity, we show a 6 to 8 times increase in spin polarization and argue that this enhancement arises from the non-uniform distribution of escape rates among molecular orbitals, resulting in better and worse conducting channels. This, combined with the alternating character of the molecular orbitals, elucidates why electron population redistribution among the channels, induced by coupling to the cavity mode, leads to a change in spin polarization. We hope that experimental verification of the proposed polarization enhancement will occur in the near future.

## 1 Introduction

Chiral-induced spin selectivity (CISS) is an effect that results in spin polarization from an electron current passing through a layer of chiral molecules. CISS was initially discovered by Ron Naaman[1], and several reviews[2–6] outline the current status of the field. CISS is at the forefront of research due to the fundamental challenges it presents to theory and its potential as a promising application tool. For instance, it plays a significant role in materials science[7,8], chemistry[9,10], and biology[11–14].

The mechanism behind the effect remains a topic of debate[15], with contributions from molecular chiral structure[16–18], spin-orbit interaction in the substrate[19], and interface characteristics[20] suggested as the origins of electron flux spin polarization. The effects of temperature[21–23] and, closely related to it, the impact of molecular vibrations[24,25] on CISS is also discussed in the literature. Finally, the connection between CISS and measurements of circularly polarized light was recently examined in ref[26].

DNA is one of the chiral molecules extensively studied within CISS research, both experimentally[1,27–29] and theoretically[16,30–37]. It is important to note that current experimental techniques enable transport measurements through both DNA layers[1] and single-molecule DNA junctions[38,39].

Development of experimental techniques at the nanoscale enables spectroscopic measurements of molecules situated within cavities. Cavity confinement leads to a strong light-matter interaction that intertwines the degrees of freedom of light and molecules, resulting in a quasiparticle known as a polariton[40]. Although light-matter interaction is significantly enhanced within the cavity, the signal from a single molecule remains relatively weak. Consequently, most experiments in molecular cavity spectroscopy are conducted on samples containing multiple molecules coupled to the cavity mode[41–51], which results in an additional scaling of the interaction on the order of $\sqrt{N}$ where $N$ represents the number of molecules in the sample. The first measurements of a single molecule in a cavity have also been documented in the literature[52,53].

Among other effects (such as the control of chemical reactions, nuclear dynamics, and energy transfer), the role of cavity confinement on electron transport is discussed in the literature. The enhancement of conductivity in organic semiconductor cavities has been measured[54], and the effect of cavity confinement on transport in single-molecule junctions has been discussed theoretically[55]. These works focus on the cavity enhancement of the charge current.

Here, we explore the potential enhancement of the CISS effect (spin current polarization) when DNA molecules are situated within a cavity. We note in passing that the coupling effect between chiral molecules and chiral cavity modes has been previously addressed in the literature and found to be negligibly small[56–58]. This is in contrast to driving by external chiral light, where enhancement of the CISS effect was reported recently[59]. For simplicity, we focus on the coupling of chiral molecules to a non-chiral cavity mode and do not consider any external driving of the system. Below, after introducing a model of the DNA cavity junction and outlining the theoretical method, we present and discuss the results of our simulations. Note that the effect of light-matter interaction considered here, while somewhat technically similar to that of electron-vibration interaction addressed in previous studies[60–62], differs in homogeneous collective coupling

[a] Department of Chemistry & Biochemistry, University of California San Diego, La Jolla, CA 92093, USA.
[b] School of Chemistry, Tel Aviv University, Tel Aviv 6997801, Israel. E-mail: mgalperin@tauex.tau.ac.il

of electronic degrees of freedom to the cavity mode vs mostly local coupling to molecular vibrations. Thus, it is natural to expect that the consequences of cavity confinement on CISS are different from those of vibrational degrees of freedom. We demonstrate that the spin polarization of the flux is sensitive to the gate voltage, and the cavity enhancement of the polarization can reach up to 6 to 8 times the value of the spin flux through the junction outside the cavity. To the best of our knowledge, the effect of light-matter interaction (cavity confinement) on CISS has not been discussed previously.

## 2 Model and Method

We consider a double-stranded DNA (dsDNA) molecule $M$ coupled to two metal electrodes, $L$ and $R$, as well as to a cavity mode $C$. The metal electrodes serve as reservoirs of free electrons, each maintaining its equilibrium. The cavity mode is represented as a harmonic oscillator. The Hamiltonian of the molecular cavity system is (here and below $\hbar = e = k_B = 1$)

$$\hat{H} = \hat{H}_M + \hat{H}_C + \hat{V}_{MC} + \sum_{K=L,R} \left(\hat{H}_K + \hat{V}_{MK}\right) \tag{1}$$

Here, $\hat{H}_M$, $\hat{H}_C$, and $\hat{H}_K$ describe isolated DNA molecule, cavity mode, and contact $K$ ($K = L,R$), respectively. $\hat{V}_{MC}$ and $\hat{V}_{MK}$ couple the subsystems.

In modeling dsDNA, we follow refs[30–32]. The explicit expression for the DNA molecule Hamiltonian is (see Figure 1)

$$\begin{aligned}\hat{H}_M = \sum_{b=1,2} \Bigg\{ \sum_{\sigma=\uparrow,\downarrow} \Bigg[ \sum_{m=1}^{N_m} \left(\varepsilon_m^{(b)} \hat{d}_{m\sigma}^{(b)\dagger} \hat{d}_{m\sigma}^{(b)} + t_m^{(b\bar{b})} \hat{d}_{m\sigma}^{(b)\dagger} \hat{d}_{m\sigma}^{(\bar{b})}\right) \\ + \sum_{m=1}^{N_m-1} \left(t_{m,m+1;\sigma}^{(b)} \hat{d}_{m\sigma}^{(b)\dagger} \hat{d}_{m+1\sigma}^{(b)} + H.c.\right) \Bigg] \\ + \sum_{\sigma,\sigma'=\uparrow,\downarrow} \sum_{m=1}^{N_m-1} \left( i t_{SO} \left[S_{m,\sigma\sigma'}^{(b)} + S_{m+1,\sigma\sigma'}^{(b)}\right] \hat{d}_{m\sigma}^{(b)\dagger} \hat{d}_{m+1\sigma'}^{(b)} + H.c.\right) \Bigg\}\end{aligned} \tag{2}$$

Here, $\hat{d}_{m\sigma}^{(b)\dagger}$ ($\hat{d}_{m\sigma}^{(b)}$) creates (annihilates) an electron with spin projection $\sigma$ on orbital $m$ of branch $b$ of the dsDNA molecule. $N_m$ is the number of monomers on each branch and $\varepsilon_m^{(b)}$ is the energy of orbital $m$ on branch $b$. Note that each monomer is represented by one orbital. $t_m^{(b\bar{b})}$ and $t_{m,m+1;\sigma}^{(b)}$ are the electron hopping matrix elements between monomers on different branches and nearest neighbor orbitals along branch $b$, respectively. $t_{SO}$ is the spin-orbit coupling (SOC) parameter and

$$S_{m,\sigma\sigma'}^{(b)} \equiv s_{\sigma\sigma'}^{z} \cos\theta - (-1)^b \left[s_{\sigma\sigma'}^{x} \sin\phi_m - s_{\sigma\sigma'}^{y} \cos\phi_m\right] \tag{3}$$

where $\mathbf{s}^{x/y/z}$ are the Pauli matrices, $\theta$ is the helix angle, $\phi_m \equiv (m-1)\Delta\phi$, and $\Delta\phi$ is the twist angle[30]. We note that spin-orbit interaction in (2) is the Rashba SOI whose expression in cylindrical coordinates was derived in ref[63].

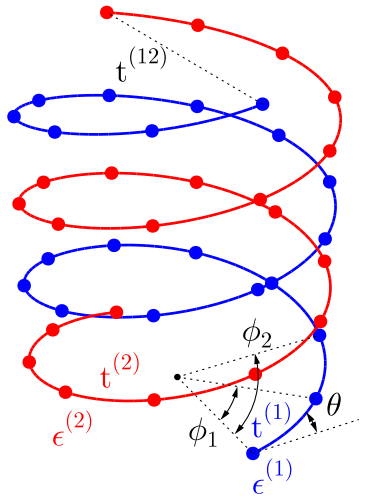


Fig. 1 Sketch of the model of the double-helix DNA.

The cavity Hamiltonian and molecule-cavity coupling are

$$\begin{aligned}\hat{H}_C &= \omega_C \hat{a}^\dagger \hat{a} \\ \hat{V}_{MC} &= -\sum_{b=1,2} \sum_{m=1}^{N_m} \sum_{\sigma=\uparrow,\downarrow} \mu_m^{(b)} E_0 \left(\hat{a} - \hat{a}^\dagger\right) \hat{d}_{m\sigma}^{(b)\dagger} \hat{d}_{m\sigma}^{(b)}\end{aligned} \tag{4}$$

Here, $\hat{a}^\dagger$ ($\hat{a}$) creates (annihilates) excitation in the cavity mode, $E_0 \equiv i\sqrt{2\pi\omega_C/V}$ is the field amplitude ($V$ is the cavity volume), and $\mu_m^{(b)} = (-1)^b \mu_0 \cos\phi_m$ ($\mu_0 = |e|R$ is a constant characterizing the molecular dipole, $e$ is the electron charge, $R$ is the radius of the DNA. Note that we describe the light-matter interaction within the standard multipolar Hamiltonian form with neglected magnetic contributions[64]. This is the form routinely used in optics. Because light (cavity mode) is treated quantum mechanically, we employ canonical quantization for the cavity mode.

Contacts Hamiltonian and molecule-contacts coupling are

$$\begin{aligned}\hat{H}_K &= \sum_{k\in K} \sum_{\sigma=\uparrow,\downarrow} \varepsilon_k \hat{c}_{k\sigma}^\dagger \hat{c}_{k\sigma} \qquad (K = L,R) \\ \hat{V}_{MK} &= \sum_{b=1,2} \sum_{k\in K} \sum_{m=1}^{N_m} \sum_{\sigma=\uparrow,\downarrow} \left(V_{mk}^{(b)} \hat{d}_{m\sigma}^{(b)\dagger} \hat{c}_{k\sigma} + H.c.\right)\end{aligned} \tag{5}$$

Here, $\hat{c}_{k\sigma}^\dagger$ ($\hat{c}_{k\sigma}$) creates (annihilates) electron with spin projection $\sigma$ in state $k$ of contact $K$. DNA is coupled to the contacts by its first and last monomers, that is

$$V_{mk}^{(b)} = \delta_{m,1} V_{Lk}^{(b)} + \delta_{m,N_m} V_{Rk}^{(b)} \tag{6}$$

Note that the model (1)-(5) can describe either single DNA molecule in a cavity or a layer of DNA molecules. In the latter case $\hat{H}_M$, eqn (2), describes the bright state and coupling $\hat{V}_{MC}$, eqn (4), has scaling factor of $\sqrt{N}$, where $N$ is number of molecules in the cavity.

Our goal is to evaluate the spin current through the DNA junction. To achieve this, we employ the standard nonequilibrium

Green's function (NEGF) approach[65,66], whose central object is the single-particle Green's function defined on the Keldysh contour as

$$G^{(bb')}_{m\sigma,m'\sigma'}(\tau,\tau') \equiv -i\langle T_c\, \hat{d}^{(b)}_{m\sigma}(\tau)\, \hat{d}^{(b')\dagger}_{m'\sigma'}(\tau')\rangle \tag{7}$$

Here, $T_c$ is the contour ordering operator, $\tau$ and $\tau'$ are contour variables, operators in the correlation function are in the Heisenberg picture, and $\langle\ldots\rangle$ is a quantum and statistical mechanics average.

Below, we will focus on the steady-state regime. Therefore, expressions are presented in terms of Fourier transforms in energy space. Dynamics of the correlation function (7) is governed by the Dyson

$$\mathbf{G}^r(E) = \left[E\mathbf{I} - \mathbf{H}_M - \Sigma^r(E)\right]^{-1} \tag{8}$$

and Keldysh

$$\mathbf{G}^{\gtrless}(E) = \mathbf{G}^r(E)\Sigma^{\gtrless}(E)\mathbf{G}^a(E) \tag{9}$$

equations. Here, $<$, $>$, $r$ and $a$ are, respectively, the lesser, greater, retarded, and advanced projections. $\mathbf{G}^a(E) = [\mathbf{G}^r(E)]^\dagger$. Non-electronic degrees of freedom (contacts and cavity mode) are taken into account via self-energies. Expression for the self-energy due to coupling to contacts is exact

$$\begin{aligned}
\Sigma^{(bb')K<}_{m\sigma,m'\sigma'}(E) &= i\delta_{\sigma,\sigma'}\Gamma^{(bb')K}_{mm'} f_K(E)\\
\Sigma^{(bb')K>}_{m\sigma,m'\sigma'}(E) &= -i\delta_{\sigma,\sigma'}\Gamma^{(bb')K}_{mm'}\left[1-f_K(E)\right]\\
\Sigma^{(bb')Kr}_{m\sigma,m'\sigma'}(E) &= -\frac{i}{2}\delta_{\sigma,\sigma'}\Gamma^{(bb')K}_{mm'}
\end{aligned} \tag{10}$$

Here, $K = L,R$, $f_K(E)$ is the Fermi-Dirac distribution,

$$\Gamma^{(bb')K}_{mm'}(E) = 2\pi\sum_{k\in K} V^{(b)}_{mk}V^{(b')}_{km'}\delta(E-\varepsilon_k), \tag{11}$$

and we assumed the wide band approximation (WBA).

The expression for self-energy due to coupling to the cavity mode is obtained from diagrammatic expansion in molecule-cavity coupling strength. In the lowest (second) order, projections of the self-energy are

$$\begin{aligned}
\Sigma^{(bb')C<}_{m\sigma,m'\sigma'}(E) &= \mu^{(b)}_m\mu^{(b')}_{m'}|E_0|^2\\
&\times\left(N_C\, G^{(bb')<}_{m\sigma,m'\sigma'}(E-\omega_C) + [1+N_C]\, G^{(bb')<}_{m\sigma,m'\sigma'}(E+\omega_C)\right)\\
\Sigma^{(bb')C>}_{m\sigma,m'\sigma'}(E) &= \mu^{(b)}_m\mu^{(b')}_{m'}|E_0|^2\\
&\times\left([1+N_C]\, G^{(bb')>}_{m\sigma,m'\sigma'}(E-\omega_C) + N_C\, G^{(bb')>}_{m\sigma,m'\sigma'}(E+\omega_C)\right)\\
\Sigma^{(bb')Cr}_{m\sigma,m'\sigma'}(E) &= i\mu^{(b)}_m\mu^{(b')}_{m'}|E_0|^2\\
&\times\int\frac{d\omega}{2\pi}\Big(\left[F^<(\omega)+F^r(\omega)\right]G^{(bb')r}_{m\sigma,m'\sigma'}(E-\omega)\\
&+F^r(\omega)\, G^{(bb')<}_{m\sigma,m'\sigma'}(E-\omega) + F^<(\omega)\, G^{(bb')r}_{m\sigma,m'\sigma'}(E+\omega)\\
&+F^a(\omega)\, G^{(bb')<}_{m\sigma,m'\sigma'}(E+\omega)\Big)
\end{aligned} \tag{12}$$

where $F^<$, $F^r$, $F^a$ are, respectively, lesser, retarded, and advanced projections of the cavity mode Green's function. Note that we neglect broadening of the cavity mode due to coupling to molecules; that is $F^<(\omega) = -2\pi i N_C\,\delta(\omega-\omega_C)$ and $F^r(\omega) = (\omega-\omega_C+i\eta)^{-1}$, where $\eta\to 0^+$, $F^a(\omega) = [F^r(\omega)]^*$, and $N_C$ is the population of the mode (the mode is assumed to be empty, with $N_C = 0$). The dependence of self-energies (12) on Green's functions $G^{(bb')}_{m\sigma,m'\sigma'}$ makes the procedure self-consistent. The procedure is assumed to be converged when elements of the electronic density matrix (given by the lesser projection of the Green's function) at consecutive iterations differ less than a predefined tolerance of $10^{-3}$.

The knowledge of the Green's function (7) allows us to simulate multiple system characteristics. Here, we are interested in simulating spin-resolved charge currents at molecule-contacts interfaces[65]

$$\begin{aligned}
I^K_\sigma = &\sum_{b,b'=1,2}\sum_{m,m'=1}^{N_m}\sum_{\sigma'=\uparrow,\downarrow}\int\frac{dE}{2\pi}\\
&\left(\Sigma^{(bb')K<}_{m\sigma,m'\sigma'}(E)\, G^{(b'b)>}_{m'\sigma',m\sigma}(E) - \Sigma^{(bb')K>}_{m\sigma,m'\sigma'}(E)\, G^{(b'b)<}_{m'\sigma',m\sigma}(E)\right)
\end{aligned} \tag{13}$$

From this expression, we define spin polarization at the interface $K$ ($L$ or $R$), $P^K_\sigma$, as

$$P^K_\sigma \equiv I^K_\sigma - I^K_{\bar\sigma} \tag{14}$$

## 3 Discussion

We now present the results of simulations. We follow refs[30–32] in the choice of parameters for the DNA junction. In particular, we consider dsDNA with $N_m = 10$ monomers, characterized by on-site energies for the two strands $\varepsilon^{(1)}_m = 0$ and $\varepsilon^{(2)}_m = 0.3\,\text{eV}$. Electron hopping parameters along the strands are $t^{(1)}_{m,m+1;\sigma} = 0.12\,\text{eV}$ and $t^{(2)}_{m,m+1;\sigma} = -0.1\,\text{eV}$. Hopping parameter between the branches is $t^{(b\bar b)}_m = -0.3\,\text{eV}$. Spin orbit coupling is $t_{SO} = 0.01\,\text{eV}$. Escape rates into contacts are $\Gamma^L = \Gamma^R = 0.05\,\text{eV}$. The distance between sites of the strand along the helix is 0.56 nm; separation along the z axis is 0.34 nm (see Figure 1 of ref[30] for a sketch). Simulations are performed at room temperature, $T = 300\,\text{K}$ for a number of Fermi energy, $E_F$, positions (gating); bias $V_{sd}$ is applied symmetrically: $\mu_{L,R} = E_F \pm eV_{sd}/2$. We consider several cavity mode frequencies, $\omega_C$, and choose light matter coupling $\mu^{(b)}_m|E_0| = 0.01\,\text{eV}$[*]

[*] Note that with DNA, the dipole radius is approximately 10 Å, estimate of its dipole moment is $\mu_0 \sim 2\,\text{D}$. So that for a typical plasmonic nanocavity, the field strength $|E_0| \sim 1\,\text{V/nm}$[67] reasonable strength of single-molecule coupling to the cavity mode is $\sim 0.2\,\text{eV}$. However, we take a smaller value of the coupling to stay within the regime of applicability of the second-order diagrammatic treatment for the light-matter interaction. Still, we get a significant enhancement of the spin polarization in the cavity. Note that the choice is still experimentally relevant because the estimate above is the maximum possible coupling; the coupling depends on several factors, including detuning of the mode from molecular resonances, the number of molecules in the sample, and the geometry of the junction itself (tilt of molecules).

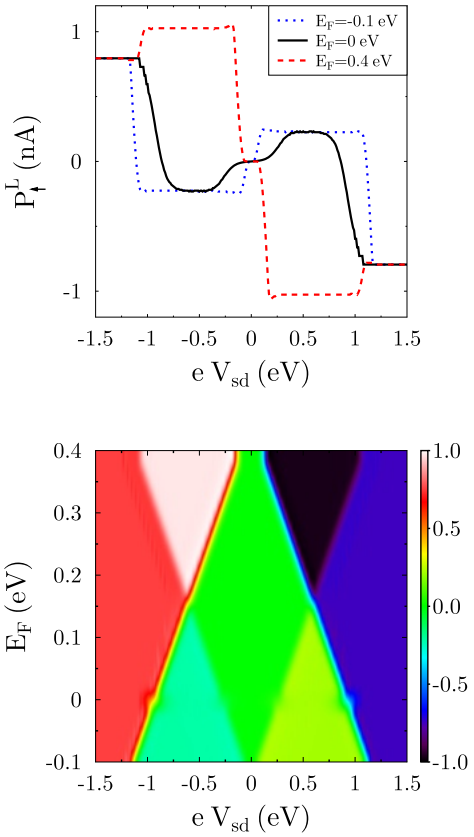


Fig. 2 Spin polarization in DNA junction at its left interface, $P^L_\uparrow$, outside of the cavity. Shown are the current vs applied bias (top panel) for three positions of Fermi energy (see inset) and current map vs bias $V_{sd}$ and Fermi energy $E_F$ position (bottom panel). See text for parameters.

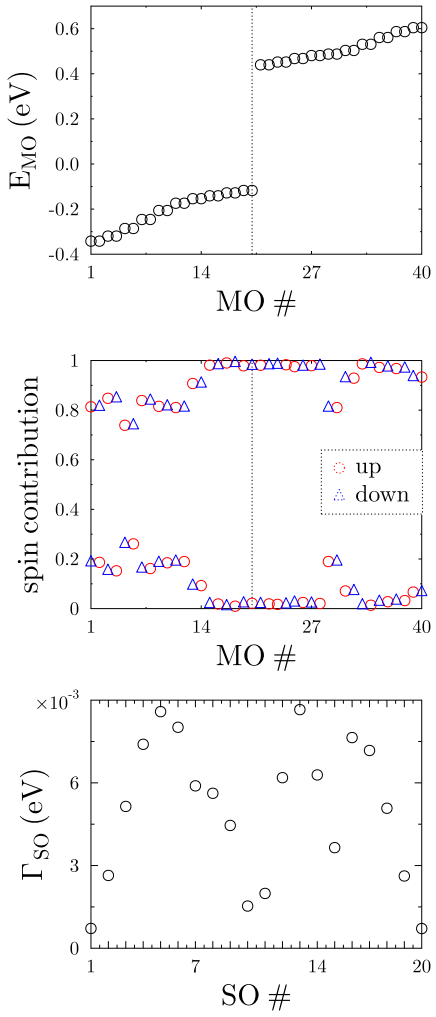


Fig. 3 Molecular orbitals of the DNA molecule. Shown are energies of the molecular orbitals (top panel), spin contributions to molecular orbitals (middle panel), and escape rates of molecular spin-orbitals (bottom panel). The dashed line in the top and middle panels indicates the position of HOMO. See text for parameters and more details.

Simulations are performed on an energy grid spanning the range from $-5$ eV to 5 eV with step 0.001 eV.

First, we consider the DNA junction outside of the cavity. Figure 2 shows spin polarization vs applied bias for a range of positions of the Fermi energy. We see that for the model the polarization is of the order of 1 nA and that it is sensitive to the gate potential.

To understand the behavior, we consider molecular orbitals (MOs) of the DNA molecule. Figure 3 shows energies of the orbitals (top panel) and spin contributions to the MOs (middle panel). We see that the dominant contribution sequentially changes from MO to its neighbor. In particular, HOMO is almost pure spin-down spin-orbital (SO), while LUMO is almost pure spin-up SO. Gating the junction we make either HOMO (for $E_F = -0.1$ eV) or LUMO (for $E_F = 0.4$ eV) dominant in contributing to the charge current, which in turn affects the spin polarization.

Now we place the DNA junction into the cavity. The top panels in Figure 4 compare polarization with and without interaction with the cavity mode of frequency $\omega_C = 0.1$ eV for three values of Fermi energy considered in the top panel of Figure 2. In the cavity, we observe a 6- to 8-fold enhancement of the spin polarization. Additionally, we observe a significant enhancement only at finite bias.

The reason for this behavior becomes clear when we compare escape rates due to coupling to contacts of different SOs (see bottom panel of Figure 3). Due to the pronounced difference in rates among SOs, scattering channels contribute differently to the charge current. We note in passing that the non-uniformity of the escape rates is not a finite-size effect: we performed calculations for 100 monomers (not shown) and the effect was preserved. Thus, the redistribution of the population from less conducting to more conducting channels increases flux. This, together with the alternating character of the MOs (see middle panel of Figure 3), explains the sensitivity of spin polarization to coupling to the cavity mode. The finite bias threshold is related to the HOMO-LUMO gap of the DNA junction (see top panel of Figure 3).

Figure 5 shows the dependence of spin polarization, eqn (14),

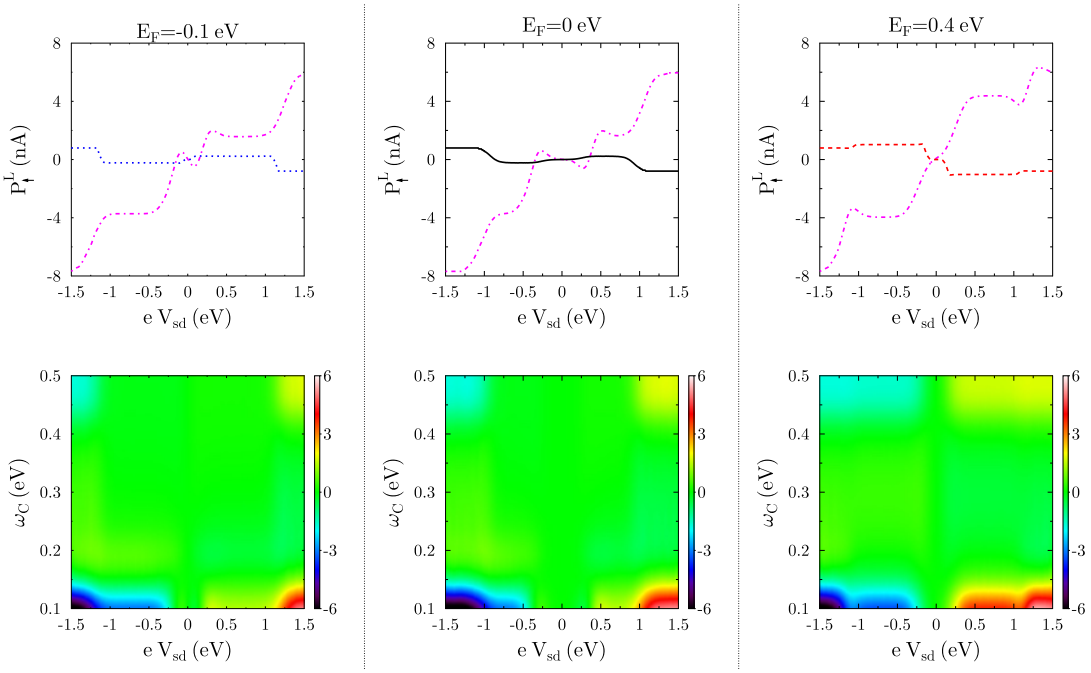


Fig. 4 Spin polarization in DNA junction at its left interface, $P^L_\uparrow$, inside cavity. The top panels compare the current inside the cavity calculated for cavity mode $w_C = 0.1$ eV (dash-dotted line, magenta) with current outside of the cavity (these results are the same as in the top panel of Figure 2). Bottom panels show current maps vs bias $V_{sd}$ and cavity mode frequency $\omega_C$. Shown are results for three positions of the Fermi energy: $E_F = -0.1$ eV (left), 0 (middle), and 0.4 eV (right). See text for parameters.

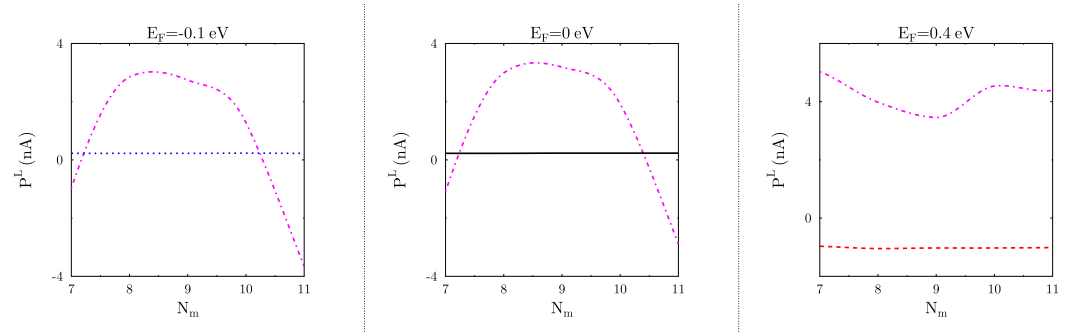


Fig. 5 Length dependence of spin polarization in DNA junction at its left interface, $P^L_\uparrow$, inside (dash-dotted line, magenta) and outside (these results are the same as in the top panel of Figure 2) of the cavity. The simulations are performed for cavity mode $w_C = 0.1$ eV at bias $V_{sd} = 0.5$ eV. Shown are results for three positions of the Fermi energy: $E_F = -0.1$ eV (left), 0 (middle), and 0.4 eV (right). See text for parameters.

on the length of the DNA (number of monomers $N_m$). We observe that outside the cavity (elastic transport), the dependence is negligible; the model yields almost the same spin selectivity for DNA junctions with $N_m = 5$ and higher. The situation drastically changes inside the cavity, where inelastic effects lead to the redistribution of spin population among conducting channels, which results in a strong non-monotonic behavior of the CISS signal.

## Conclusions

In conclusion, utilizing a model of the double-stranded DNA junction, we investigated the chiral-induced spin selectivity effect both outside and inside the molecular cavity. We demonstrated that outside the cavity, spin polarization is sensitive to gate voltage, attributing this sensitivity to the alternating character of DNA molecular orbitals. With the HOMO being predominantly spin-down and the LUMO predominantly spin-up, the molecular orbitals that dominate charge transport dictate spin polarization. Inside the cavity, we observed a 6- to 8-fold increase in spin polarization.

We contend that this enhancement arises from the non-uniform distribution of escape rates among molecular orbitals, leading to varying conducting channels. This, combined with the alternating character of the molecular orbitals, elucidates why electron population redistribution among the channels results in a change in polarization. We anticipate that experimental verification of the proposed polarization enhancement will occur soon.

## Author contributions

A. Li: investigation, writing–reviewing and editing; M. Galperin: conceptualization, investigation, formal analysis, visualization, writing–original draft preparation, writing–reviewing and editing.

## Conflicts of interest

There are no conflicts to declare.

## Acknowledgements

Research of A.L. is supported by the NSF Grant No. CHE-2154323.

## Notes and references

1 K. Ray, S. P. Ananthavel, D. H. Waldeck and R. Naaman, *Science*, 1999, **283**, 814–816.
2 R. Naaman, *Isr. J. Chem.*, 2016, **56**, 1010–1015.
3 J. E. Subotnik, *Science*, 2023, **382**, 160–161.
4 B. P. Bloom, Y. Paltiel, R. Naaman and D. H. Waldeck, *Chem. Rev.*, 2024, **124**, 1950–1991.
5 R. Naaman and D. H. Waldeck, *J. Phys. Chem. Lett.*, 2024, **15**, 11002–11006.
6 R. Naaman, J. E. Subotnik and D. H. Waldeck, *J. Chem. Phys.*, 2024, **160**, 096101.
7 A. K. Mondal, N. Brown, S. Mishra, P. Makam, D. Wing, S. Gilead, Y. Wiesenfeld, G. Leitus, L. J. W. Shimon, R. Carmieli, D. Ehre, G. Kamieniarz, J. Fransson, O. Hod, L. Kronik, E. Gazit and R. Naaman, *ACS Nano*, 2020, **14**, 16624–16633.
8 D. H. Waldeck, R. Naaman and Y. Paltiel, *APL Materials*, 2021, **9**, 040902.
9 R. Naaman, Y. Paltiel and D. H. Waldeck, *Acc. Chem. Res.*, 2020, **53**, 2659–2667.
10 A. Stefani, A. Bogdan, F. Pop, F. Tassinari, L. Pasquali, C. Fontanesi and N. Avarvari, *J. Chem. Phys.*, 2023, **159**, 204706.
11 R. Naaman and D. Waldeck, *Inference*, 2017, **3**, year.
12 R. Naaman, Y. Paltiel and D. H. Waldeck, *Annu. Rev. Biophys.*, 2022, **51**, 99–114.
13 Y. Kapon, Q. Zhu, S. Yochelis, R. Naaman, R. Gutierrez, G. Cuniberti, Y. Paltiel and V. Mujica, *J. Chem. Phys.*, 2023, **159**, 224702.
14 C. M. Niman, N. Sukenik, T. Dang, J. Nwachukwu, M. A. Thirumurthy, A. K. Jones, R. Naaman, K. Santra, T. K. Das, Y. Paltiel, L. T. Baczewski and M. Y. El-Naggar, *J. Chem. Phys.*, 2023, **159**, 145101.
15 F. Evers, A. Aharony, N. Bar-Gill, O. Entin-Wohlman, P. Hedegøard, O. Hod, P. Jelinek, G. Kamieniarz, M. Lemeshko, K. Michaeli, V. Mujica, R. Naaman, Y. Paltiel, S. Refaely-Abramson, O. Tal, J. Thijssen, M. Thoss, J. M. van Ruitenbeek, L. Venkataraman, D. H. Waldeck, B. Yan and L. Kronik, *Adv. Mater.*, 2022, **34**, 2106629.
16 Y. Utsumi, O. Entin-Wohlman and A. Aharony, *Phys. Rev. B*, 2020, **102**, 035445.
17 P. Hedegøard, *J. Chem. Phys.*, 2023, **159**, 104104.
18 J. M. van Ruitenbeek, R. Korytár and F. Evers, *J. Chem. Phys.*, 2023, **159**, 024710.
19 J. Gersten, K. Kaasbjerg and A. Nitzan, *J. Chem. Phys.*, 2013, **139**, 114111.
20 Y. Dubi, *Chem. Sci.*, 2022, **13**, 10878–10883.
21 T. K. Das, F. Tassinari, R. Naaman and J. Fransson, *J. Phys. Chem. C*, 2022, **126**, 3257–3264.
22 J. Fransson, *J. Chem. Phys.*, 2023, **159**, 084115.
23 S. Alwan, S. Sarkar, A. Sharoni and Y. Dubi, *J. Chem. Phys.*, 2023, **159**, 014106.
24 A. Kato, H. M. Yamamoto and J.-i. Kishine, *Phys. Rev. B*, 2022, **105**, 195117.
25 S. Miwa, T. Yamamoto, T. Nagata, S. Sakamoto, K. Kimura, M. Shiga, W. Gao, H. M. Yamamoto, K. Inoue, T. Takenobu, T. Nozaki and T. Ohto, *Spin polarization driven by molecular vibrations leads to enantioselectivity in chiral molecules*, 2024.
26 C. Climent, E. J. Schelter, D. H. Waldeck, S. A. Vinogradov and J. E. Subotnik, *J. Chem. Phys.*, 2023, **159**, 134304.
27 R. Naaman and D. H. Waldeck, *J. Phys. Chem. Lett.*, 2012, **3**, 2178–2187.
28 R. Naaman, Y. Paltiel and D. H. Waldeck, *Nat. Rev. Chem.*, 2019, **3**, 250–260.
29 Q. Zhu, Y. Kapon, A. M. Fleming, S. Mishra, K. Santra, F. Tassinari, S. R. Cohen, T. K. Das, Y. Sang, D. K. Bhowmick, C. J. Burrows, Y. Paltiel and R. Naaman, *Cell Rep. Phys. Sci.*, 2022, **3**, 101157.
30 A.-M. Guo and Q.-f. Sun, *Phys. Rev. Lett.*, 2012, **108**, 218102.

31 A.-M. Guo and Q.-f. Sun, *Phys. Rev. B*, 2012, **86**, 035424.

32 D. Rai and M. Galperin, *J. Phys. Chem. C*, 2013, **117**, 13730–13737.

33 S. Matityahu, Y. Utsumi, A. Aharony, O. Entin-Wohlman and C. A. Balseiro, *Phys. Rev. B*, 2016, **93**, 075407.

34 P.-J. Hu, S.-X. Wang, X.-H. Gao, Y.-Y. Zhang, T.-F. Fang, A.-M. Guo and Q.-F. Sun, *Phys. Rev. B*, 2020, **102**, 195406.

35 Y. Liu, J. Xiao, J. Koo and B. Yan, *Nature Materials*, 2021, **20**, 638–644.

36 L. Deng, I. H. Bhat and A.-M. Guo, *J. Chem. Phys.*, 2023, **158**, 244116.

37 N. Bangruwa, Suryansh, M. Peralta, R. Gutierrez, G. Cuniberti and D. Mishra, *J. Chem. Phys.*, 2023, **159**, 044702.

38 D. Porath, A. Bezryadin, S. de Vries and C. Dekker, *Nature*, 2000, **403**, 635–638.

39 H. Cohen, C. Nogues, R. Naaman and D. Porath, *PNAS*, 2005, **102**, 11589–11593.

40 T. E. Li, B. Cui, J. E. Subotnik and A. Nitzan, *Annu. Rev. Phys. Chem.*, 2022, **73**, 43–71.

41 T. Schwartz, J. A. Hutchison, C. Genet and T. W. Ebbesen, *Phys. Rev. Lett.*, 2011, **106**, 196405.

42 J. A. Hutchison, T. Schwartz, C. Genet, E. Devaux and T. W. Ebbesen, *Angew. Chem. Int. Ed.*, 2012, **51**, 1592–1596.

43 J. A. Hutchison, A. Liscio, T. Schwartz, A. Canaguier-Durand, C. Genet, V. Palermo, P. Samorì and T. W. Ebbesen, *Adv. Mater.*, 2013, **25**, 2481–2485.

44 T. Schwartz, J. A. Hutchison, J. Léonard, C. Genet, S. Haacke and T. W. Ebbesen, *ChemPhysChem*, 2013, **14**, 125–131.

45 A. W. Eddins, C. C. Beedle, D. N. Hendrickson and J. R. Friedman, *Phys. Rev. Lett.*, 2014, **112**, 120501.

46 E. Eizner, K. Akulov, T. Schwartz and T. Ellenbogen, *Nano Lett.*, 2017, **17**, 7675–7683.

47 G. G. Rozenman, K. Akulov, A. Golombek and T. Schwartz, *ACS Photonics*, 2018, **5**, 105–110.

48 K. Akulov, D. Bochman, A. Golombek and T. Schwartz, *J. Phys. Chem. C*, 2018, **122**, 15853–15860.

49 B. Xiang, R. F. Ribeiro, M. Du, L. Chen, Z. Yang, J. Wang, J. Yuen-Zhou and W. Xiong, *Science*, 2020, **368**, 665–667.

50 T.-T. Chen, M. Du, Z. Yang, J. Yuen-Zhou and W. Xiong, *Science*, 2022, **378**, 790–794.

51 Z. Yang and W. Xiong, *Adv. Quantum Technol.*, 2022, **5**, 2100163.

52 R. Chikkaraddy, B. de Nijs, F. Benz, S. J. Barrow, O. A. Scherman, E. Rosta, A. Demetriadou, P. Fox, O. Hess and J. J. Baumberg, *Nature*, 2016, **535**, 127–130.

53 F. Benz, M. K. Schmidt, A. Dreismann, R. Chikkaraddy, Y. Zhang, A. Demetriadou, C. Carnegie, H. Ohadi, B. de Nijs, R. Esteban, J. Aizpurua and J. J. Baumberg, *Science*, 2016, **354**, 726–729.

54 E. Orgiu, J. George, J. A. Hutchison, E. Devaux, J. F. Dayen, B. Doudin, F. Stellacci, C. Genet, J. Schachenmayer, C. Genes, G. Pupillo, P. Samorì and T. W. Ebbesen, *Nat. Mater.*, 2015, **14**, 1123–1129.

55 D. Hagenmüller, J. Schachenmayer, S. Schütz, C. Genes and G. Pupillo, *Phys. Rev. Lett.*, 2017, **119**, 223601.

56 K. Voronin, A. S. Taradin, M. V. Gorkunov and D. G. Baranov, *ACS Photonics*, 2022, **9**, 2652–2659.

57 C. Schäfer and D. G. Baranov, *J. Phys. Chem. Lett.*, 2023, **14**, 3777–3784.

58 L. M. Tomasch, F. Spallek, G. W. Fuchs, T. F. Giesen and S. Y. Buhmann, *Strong coupling of a chiral molecule with circularly polarised modes inside a cavity*, 2024.

59 W. Liu, J. Chen and W. Dou, *J. Phys. Chem. C*, 2025, **129**, 10181–10188.

60 J. Fransson, *Phys. Rev. B*, 2020, **102**, 235416.

61 G.-F. Du, H.-H. Fu and R. Wu, *Phys. Rev. B*, 2020, **102**, 035431.

62 R. Smorka, S. L. Rudge and M. Thoss, *J. Chem. Phys.*, 2025, **162**, 014304.

63 Q.-f. Sun, X. C. Xie and J. Wang, *Phys. Rev. B*, 2008, **77**, 035327.

64 S. Mukamel, *Principles of Nonlinear Optical Spectroscopy*, Oxford University Press, 1995.

65 H. Haug and A.-P. Jauho, *Quantum Kinetics in Transport and Optics of Semiconductors*, Springer, Berlin Heidelberg, 2nd edn, 2008.

66 G. Stefanucci and R. van Leeuwen, *Nonequilibrium Many-Body Theory of Quantum Systems. A Modern Introduction.*, Cambridge University Press, Cambridge, 2nd edn, 2025.

67 X. Zheng, Q. Pei, J. Tan, S. Bai, Y. Luo and S. Ye, *Chem. Sci.*, 2024, **15**, 11507–11514.